# Density Functional Study of the Interfacial Electron Transfer Pathway for Monolayer-Adsorbed InN on the TiO 2 Anatase (101) Surface

**ARTICLE** *in* THE JOURNAL OF PHYSICAL CHEMISTRY B · DECEMBER 2006

Impact Factor: 3.3 · DOI: 10.1021/jp061975u · Source: PubMed



**6 AUTHORS**, INCLUDING:

jyh shing Lin
Tamkang University
**44** PUBLICATIONS **1,633** CITATIONS
SEE PROFILE

Shao yu Lu
Tamkang University
**7** PUBLICATIONS **19** CITATIONS
SEE PROFILE

Yung-Ting Lee
Korea Advanced Institute of Science and Tec…
**4** PUBLICATIONS **14** CITATIONS
SEE PROFILE

# Density Functional Study of the Interfacial Electron Transfer Pathway for Monolayer-Adsorbed InN on the $TiO_2$ Anatase (101) Surface

**Jyh Shing Lin,* Wen-Chi Chou,*,† Shao-Yu Lu, Geng-Jya Jang, Bo-Rong Tseng, and Yung-Ting Li**

*Department of Chemistry, Tamkang University, Tamsui, Taiwan*

*Received: March 30, 2006; In Final Form: September 2, 2006*

Density functional theory (DFT) in connection with ultrasoft pseudopotential (USP) and generalized gradient spin-polarized approximations (GGSA) is applied to calculate the adsorption energies and structures of monolayer-adsorbed InN on the $TiO_2$ anatase (101) surface and the corresponding electronic properties, that is, partial density of states (PDOS) for surface and bulk layers of the $TiO_2$ anatase (101) surface and monolayer-adsorbed InN, to shed light on the possible structural modes for initial photoexcitation within the UV/vis adsorption region followed by fast electron injection through the InN/$TiO_2$ interface for an InN/$TiO_2$-based solar cell design. Our calculated adsorption energies found that the two most probable stable structural modes of monolayer-adsorbed InN on the $TiO_2$ anatase (101) surface are (1) an end-on structure with an adsorption energy of 2.52 eV through N binding to surface 2-fold coordinated O ($O_{cn2}$), that is, InN−$O_{cn2}$, and (2) a side-on structure with an adsorption energy of 3.05 eV through both N binding to surface 5-fold coordinated Ti ($Ti_{cn5}$) and In bridging two surface $O_{cn2}$, that is, $(O_{cn2})_2$−InN−$Ti_{cn5}$. Our calculated band gaps for both InN−$O_{cn2}$ and $(O_{cn2})_2$−InN−$Ti_{cn5}$ (including a 1.0-eV correction using a scissor operator) of monolayer-adsorbed InN on the $TiO_2$ anatase (101) surface are red-shifted to 1.7 eV (730 nm) and 2.3 eV (540 nm), respectively, which are within the UV/vis adsorption region similar to Gratzel's black dye solar cell. Our analyses of calculated PDOS for both surface and bulk layers of the $TiO_2$ anatase (101) surface and monolayer-adsorbed InN on the $TiO_2$ anatase (101) surface suggest that the $(O_{cn2})_2$−InN−$Ti_{cn5}$ configuration of monolayer-adsorbed InN on the $TiO_2$ anatase (101) surface would provide a more feasible structural mode for the electron injection through the InN/$TiO_2$ interface. This is due to the presence of both occupied and unoccupied electronic states for monolayer-adsorbed InN within the band gap $TiO_2$ anatase (101) surface, which will allow the photoexcitation within the UV/vis adsorption region to take place effectively, and subsequently the photoexcited electronic states will overlap with the unoccupied electronic states around the lowest conduction band of the $TiO_2$ anatase (101) surface, which will ensure the electron injection through the InN/$TiO_2$ interface. Finally, another thing worth our attention is our preliminary study of double-layer-adsorbed InN on the $TiO_2$ anatase (101) surface, that is, $(O_{cn2})_2$−$(InN)_2$−$Ti_{cn5}$, with a calculated band gap red-shifted to 2.6 eV (477 nm) and a different overlap of electronic states between double-layer-adsorbed InN and the $TiO_2$ anatase (101) surface qualitatively indicated that there is an effect of the thickness of adsorbed InN on the $TiO_2$ anatase (101) surface on both photoexcitation and electron injection processes involved in the photoinduced interfacial electron transfer through InN/$TiO_2$. A more thorough and comprehensive study of different layers of InN adsorbed in all possible different orientations on the $TiO_2$ anatase (101) surface is presently in progress.

## Introduction

During the past decade, the sensitization of nanocrystalline $TiO_2$ particles by adsorbed dyes[1−6] and polymers[7,8] has been studied extensively with the aim of obtaining higher solar energy conversion through the photovoltaic effect. However, dyes are very expensive, and organic compounds have shorter lifetimes and are less stable than inorganic materials such as semiconductors. Therefore, alternative studies[9−12] of the sensitization of nanocrystalline $TiO_2$ by different quantum-sized InP, PbS, CdS, and $Ag_2S$ were carried out simultaneously to demonstrate their potential as good candidates for providing better photoinduced electron transfer from these quantum-sized semiconductors to nanocrystalline $TiO_2$. From these studies, it is generally accepted that these special chosen sensitizers after adsorption onto the nanocrystalline $TiO_2$ must possess a suitable band gap to adsorb sunlight effectively and that they also have to directly involve generating a suitable conduction band edge through which the electronic interaction between these special chosen sensitizers and nanocrystalline $TiO_2$ will occur for rapidly transferring photoinduced electrons.

Recently, M. C. Lin and his colleague successfully demonstrated[13] the deposition of high-quality InN films with varying thickness onto nanocrystalline $TiO_2$ using trimethyl indium (TMIn) and hydrazoic acid ($HN_3$) by low-pressure organometallic chemical vapor deposition (OMCVD). They also identified the most observed orientation of the deposited InN films and two different phases of the $TiO_2$ nanoparticles, that is, anatase and rutile, using X-ray powder diffractometry (XRD). Finally, they illustrated the resulting InN film on $TiO_2$ by exhibiting a broad UV/vis absorption between 390 and 800 nm quite similar to Gratzel's "black" dye. To extend their insight into the structural and electronic properties of InN-sensitized $TiO_2$ nanoparticle films, they also applied the ultrasoft pseudopotential

* Corresponding authors.
† Fax: +886-2-26209924. E-mail: 892170027@s92.tku.edu.tw.

10.1021/jp061975u CCC: $33.50 
Published on Web 10/26/2006

total energy calculation based on density functional theory to investigate the structural properties of monolayer-adsorbed InN on both $TiO_2$ rutile (110) and anatase (101) surfaces.[14] Furthermore, they calculated the band gaps for these structures of monolayer-adsorbed InN on both surfaces, and they suggested that there are no significant differences between the clean surfaces and the monolayer-adsorbed InN on both surfaces[14] without further explanation.

However, their computational work does not involve the study of the electronic properties of the monolayer-adsorbed InN on both $TiO_2$ rutile (110) and anatase (101) surfaces during the process of the photoexcitation of monolayer-adsorbed InN followed by interfacial electron transfer through the InN/$TiO_2$ interface. Particularly, the knowledge of both the highest occupied electronic states and lowest unoccupied electronic states of monolayer-adsorbed InN and the unoccupied electronic states around the lowest conduction band of both $TiO_2$ rutile (110) and anatase (101) surfaces is crucial to rationalize the electron-transfer pathway for effective solar energy conversion. Consequently, it is necessary to establish the energy diagrams for monolayer-adsorbed InN on both $TiO_2$ rutile (110) and anatase (101) surfaces upon which the photoexcitation of monolayer-adsorbed InN followed by the electron injection into the lowest conduction band of the $TiO_2$ anatase (101) surface will be based.

A few years ago we performed total energy calculations based on density functional theory to study the structural and electronic properties of adsorbed silane on both Si(100) and Ge(100) surfaces.[15,16] To realize the different electronic states from these two surfaces and their effects on the $SiH_4$ adsorption reaction mechanisms, we also calculated the PDOS for the surface layer of both surfaces. Indeed, these calculated PDOS showed that the higher electronic states from both surfaces play an important role in governing the reactivity for the $SiH_4$ adsorption reaction on these two surfaces. These studies encouraged us to use the calculated PDOS of the monolayer-adsorbed InN and $TiO_2$ anatase (101) surface layer to establish an energy diagram for illustrating the photoinduced electron transfer for monolayer-adsorbed InN on the $TiO_2$ anatase (101) surface through the photoexcitation of adsorbed InN followed by the electron injection into the lowest conduction band of the $TiO_2$ anatase (101) surface. In this paper, we therefore employed ab-initio ultrasoft pseudopotential total energy calculations with generalized gradient spin-polarized approximations (GGSA) to calculate the structural properties for monolayer-adsorbed InN on the $TiO_2$ anatase (101) surface. In particular, we will focus on the stability of different structural modes of monolayer-adsorbed InN on the $TiO_2$ anatase (101) surface. Then we will calculate the partial density of states (PDOS) (1) for both surface and bulk layers of $TiO_2$ anatase (101) surfaces, and (2) for more stable structural modes of monolayer-adsorbed InN on the $TiO_2$ anatase (101) surface to illustrate the nature of these electronic states and their involvement in both photoexcitation and electron injection processes for better insight into the photoinduced interfacial electron transfer through the InN/$TiO_2$ interface. Finally, we present our preliminary calculated results of double-layer-adsorbed InN on the$TiO_2$ anatase (101) surface, that is, $(O_{cn2})_2-(InN)_2-Ti_{cn5}$, to illustrate the effect of the thickness of adsorbed InN on the $TiO_2$ anatase (101) surface on the electronic properties mentioned above in the hope of complementing the experimental data[13] described above.

## Computational Methods

Our computational strategy is to perform all calculations using a periodic boundary condition with an electronic orbital represented by using plane-wave basis sets. We have used the density-mixing scheme described by Kresse and Furthmuller[17] to effectively reach self-consistency for the Kohn−Sham energy functional in which the generalized gradient spin-polarized approximation (GGSA) of Perdew and Wang[18] is utilized. The ultrasoft pseudopotential based on the Vanderbilt method of ultrasoft pseudopotential generation[19] describes the interactions between the ions and electrons. A Kleinman−Bylander representation[20] of the ultrasoft pseudopotential is automatically introduced due to its construction. This allows the plane-wave matrix elements of the ultrasoft pseudopotential to be expressed in a separable form for computational efficiency. In our calculations, only the $TiO_2$ anatase (101) surface is considered to illustrate the possible energy diagrams arising from different thermally stable configurations of monolayer-adsorbed InN on this surface. The $TiO_2$ anatase (101) surface is represented by periodically repeated slabs of $TiO_2$ layers with bond lengths and angles based on the experimental result. The lower part of the slab is fixed as the bulk-truncated structure and a certain vacuum region approximately 10 Å is used to separate the top and bottom surfaces of the slab to avoid interaction between distinct slab surfaces in this infinitely periodic model system. We also explored the convergence test by calculating the lattice parameters of bulk $TiO_2$ crystals of the anatase phase within 2% error with a cutoff of 650 eV and 43 Monkhorst−Pack special *k*-points. Therefore, the above cutoff and Monkhorst−Pack special *k*-points are used throughout all the calculations.[21] To obtain the PDOS, we generated the total density of states (TDOS) of the whole system using a reasonable number of *k*-points and bands (normally a few more than the occupied bands). Then we decomposed the TDOS into the contribution of partial fragments, that is, the surface layer, bulk layer, and monolayer-adsorbed molecule, of those selected bands to give rise to the PDOS. Here, we have to introduce the space cut for each atomic component of partial fragments to exclude the unnecessary contribution from other neighboring atoms. In this study, we consider Ti, O, In, and N as the constituent atoms to generate the PDOS, and their space cuts are chosen as their covalent radii, respectively. Technical details about our total energy calculation method, the ultrasoft pseudopotential generation scheme, and the PDOS calculation scheme have been reported elsewhere.[15] We performed all the total energy and PDOS calculations using a modified version of CASTEP 3.9.[22]

## Calculated Results and Discussions

**Surface and Electronic Structures of $TiO_2$ Anatase (101).** To obtain the possible structural modes of monolayer-adsorbed InN on the $TiO_2$ anatase (101) surface, we will first investigate the relaxed $TiO_2$ anatase (101) surface structure. On the basis of our calculated results, we found that both 5-fold coordinated Ti atoms and 2-fold coordinated O atoms ($Ti_{cn5}$ and $O_{cn2}$) are present on the first layer of the surface layer and also there are both 6-fold coordinated Ti atoms and 3-fold coordinated O atoms ($Ti_{cn6}$ and $O_{cn3}$) on the second layer of the surface layer as shown in Figure 1. These atoms on this relaxed surface are only slightly displaced from their ideal bulk positions. The coordinatively unsaturated $O_{cn2}$ and $Ti_{cn5}$ atoms tend to tighten their bonds with nearest neighbors and relaxed inward by 0.09 and 0.04 Å, respectively. However, both $O_{cn3}$ and $Ti_{cn6}$ atoms relaxed outward by 0.34 and 0.25 Å, respectively. Finally, the distance between $O_{cn2}$ and $Ti_{cn5}$ atoms is only slightly elongated by 0.04 Å after relaxation which, we believe, will have very little effect on the electronic properties, that is, band gaps, as compared with those of the anatase $TiO_2$ bulk structure.

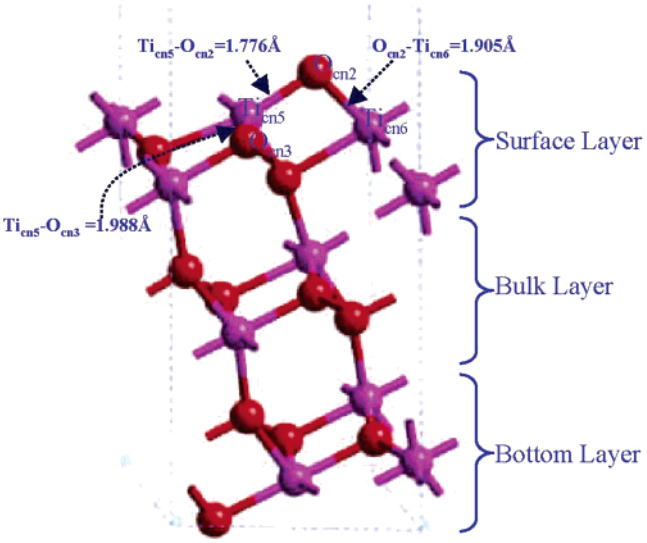


**Figure 1.** Side view of the relaxed $TiO_2$ anatase (101) surface structure.

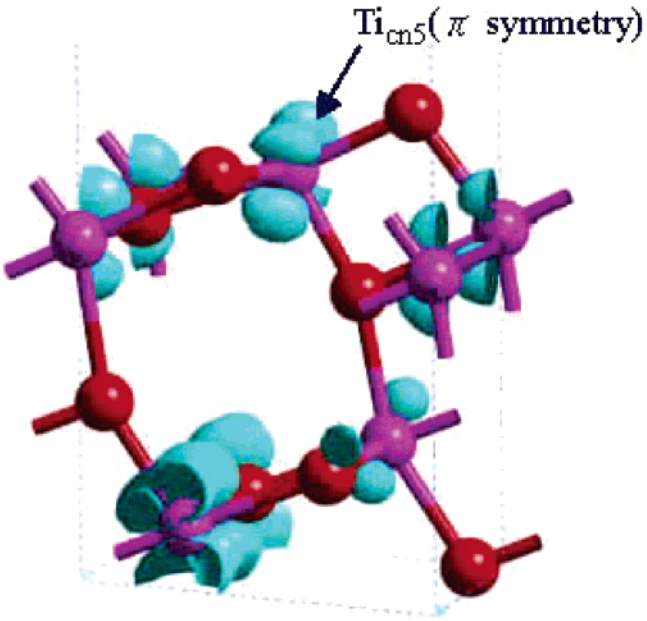


**Figure 2.** The calculated electron density at the lowest conduction band of the $TiO_2$ anatase (101) surface.

Following the brief description of the relaxed $TiO_2$ anatase (101) surface structure above, we are now in a position to rationalize its corresponding electronic property in order to understand the possible structural modes of monolayer-adsorbed InN on the $TiO_2$ anatase (101) surface and their possible interfacial electron transfer pathways. As mentioned earlier, there are coordinatively unsaturated $Ti_{cn5}$ and $O_{cn2}$ atoms on the first layer of this relaxed surface. Therefore, our calculated PDOS for the first layer of the $TiO_2$ anatase (101) surface would reflect the possible electronic properties of both $Ti_{cn5}$ and $O_{cn2}$ atoms to (1) provide the possible structural modes of monolayer-adsorbed InN on the $TiO_2$ anatase (101) surface, and (2) estimate the corresponding band gap for sensible photoexcitation within the UV/vis adsorption region. Indeed, we found that there is a $\pi$-characteristic of $Ti_{cn5}$ at the lowest conduction band of the $TiO_2$ anatase (101) surface (as shown in Figure 2) based on our calculated electron density, and there are some noticeable electronic states of $O_{cn2}$ below the Fermi level based on our calculated PDOS of $O_{cn2}$ on the first layer of the $TiO_2$ anatase (101) surface (as shown in Figure 3). In addition, we estimated the band gap of the $TiO_2$ anatase (101) surface on the basis of our calculated PDOS of $Ti_{cn5}$ with a 1-eV correction obtained from the calculated underestimated indirect band gap of the $TiO_2$ anatase bulk structure as shown in Figure 4 using a scissor operator due to the density functional approximation. In consequence, our estimated band gap of the $TiO_2$ anatase (101) surface is around 3.2 eV (as shown in Figure 3) and is almost the same as that of the anatase $TiO_2$ bulk structure as we expected in our earlier discussion. Finally, these electronic properties of the $TiO_2$ anatase (101) surface clearly provide guidance for not only obtaining the possible structural modes of monolayer-adsorbed InN on the $TiO_2$ anatase (101) surface but also qualitatively evaluating their possible interfacial electron-transfer pathways through InN/$TiO_2$ after the photoexcitation within the UV/vis adsorption region. The details will be discussed in later sections.

**Different Structural Modes of Monolayer-Adsorbed InN on the $TiO_2$ Anatase (101) Surface.** Having realized that there is a $\pi$-characteristic of $Ti_{cn5}$ around the lowest conduction band and that there are noticeable electronic states of $O_{cn2}$ below the Fermi level for the $TiO_2$ anatase (101) surface mentioned in the previous section, we easily appreciate their involvement in order to provide the feasible structural mode of monolayer-adsorbed InN on the $TiO_2$ anatase (101) surface for the interfacial electron transfer through InN/$TiO_2$. To elaborate this in detail, we first realized on the basis of our calculated PDOS that the electron injection from monolayer-adsorbed InN to the $TiO_2$ anatase (101) surface could only take place through the photoexcited state of monolayer-adsorbed InN to the unoccupied electronic states around the lowest conduction band of the $TiO_2$ anatase (101) surface. Furthermore, it is known from the recent calculated results[14] that the N atom within InN will form a strong bond with either $O_{cn2}$ or Ti $_{cn5}$ to have an end-on adsorbed InN on the $TiO_2$ anatase (101) surface. Finally, we have to demand that the structural modes for monolayer-adsorbed InN on the $TiO_2$ anatase (101) surface have to be thermodynamically stable to provide the steady channel for the interfacial electron transfer through InN/$TiO_2$. Following these arguments, we proposed that one of the possible stable structural modes of monolayer-adsorbed InN on the $TiO_2$ anatase (101) surface is the end-on structure, that is, InN−$O_{cn2}$, through N binding to surface $O_{cn2}$. Indeed, our calculated InN−$O_{cn2}$ as shown in Figure 5 is thermodynamically stable by 2.52 eV. It is almost 0.88 eV more stable than that from ref 14.

We further proposed another possible structural mode of monolayer-adsorbed InN on the anatase $TiO_2$ (101) surface that is the end-on structure, that is, InN−$Ti_{cn5}$, through N binding to surface $Ti_{cn5}$. Unexpectedly, we obtained a thermodynamically more stable side-on adsorption structure, that is, $(O_{cn2})_2$−InN−$Ti_{cn5}$; even we expected to find an end-on structure, that is, InN−$Ti_{cn5}$. Our calculated $(O_{cn2})_2$−InN−$Ti_{cn5}$ as shown in Figure 6 is thermodynamically stable by 3.05 eV and is nearly 1.59 eV more stable than the calculated InN−$Ti_{cn5}$ in ref 14. We attribute this extra stability to the bridging interaction between In and $(O_{cn2})_2$ atoms. All other structural modes of monolayer adsorbed InN on the $TiO_2$ anatase (101) surface as described in ref 14 are not considered due to the fact that they are much less stable in comparison with these two structural modes, that is, InN−$O_{cn2}$ and $(O_{cn2})_2$−InN−$Ti_{cn5}$, mentioned above. Consequently, they are unlikely to behave as steady modes for the interfacial electron transfer through InN/$TiO_2$.

**Possible Interfacial Electron-Transfer Pathway for Monolayer-Adsorbed InN on the $TiO_2$ Anatase (101) Surface.** Despite its great technological significance, the interfacial

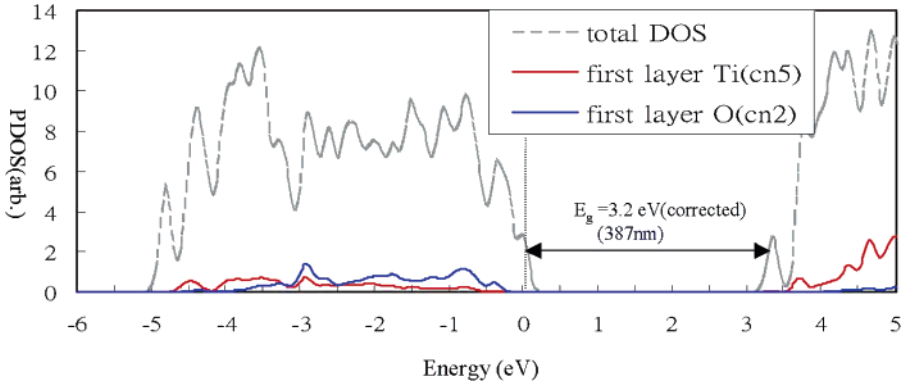


**Figure 3.** The calculated PDOS of the first layer, that is, $Ti_{cn5}$ and $O_{cn2}$, of the $TiO_2$ anatase (101) surface as shown by the red line and the blue line, respectively.

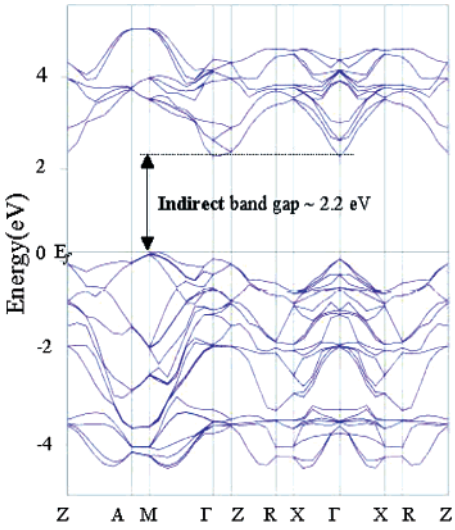


**Figure 4.** The calculated band structure of $TiO_2$ anatase bulk along selected symmetry directions.

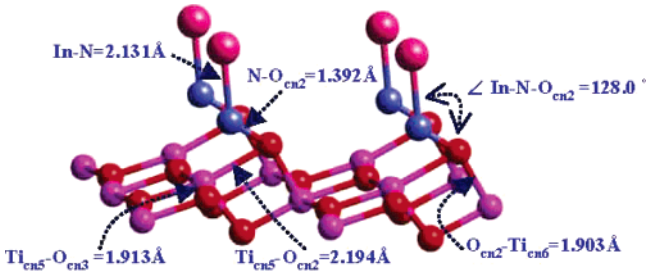


**Figure 5.** The calculated end-on structure mode of monolayer-adsorbed InN on the $TiO_2$ anatase (101) surface, that is, InN−$O_{cn2}$.

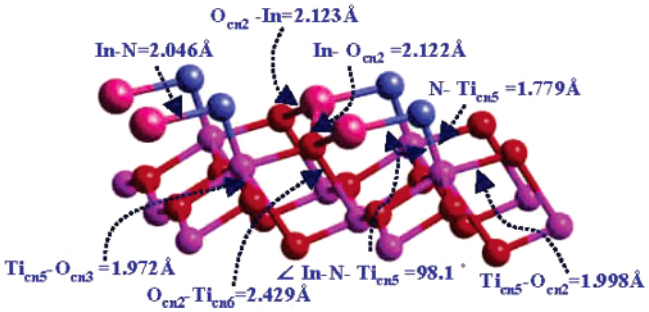


**Figure 6.** The calculated side-on structure mode of monolayer-adsorbed InN on the $TiO_2$ anatase (101) surface, that is, $(O_{cn2})_2$−InN−$Ti_{cn5}$.

electron-transfer pathway between adsorbed InN and the $TiO_2$ anatase (101) surface of an InN/$TiO_2$ solar cell still remains poorly understood. As we already discussed earlier, the calculated electronic properties of the $TiO_2$ anatase (101) surface could provide the guidance for the possible stable structural modes of monolayer-adsorbed InN on the $TiO_2$ anatase (101) surface. Furthermore, these calculated electronic properties of these different stable structural modes of monolayer-adsorbed InN on the $TiO_2$ anatase (101) surface can easily establish the energy diagram to qualitatively manifest both photoexcitation and electron injection processes for possible interfacial electron transfer through InN/$TiO_2$. To elaborate this in detail, we first calculated the PDOS for monolayer-adsorbed InN and both surface and bulk layers for the $TiO_2$ anatase (101) surface as indicated in Figure 1. Then we will estimate the variation of their band gaps in comparison with that of the clear $TiO_2$ anatase (101) surface to determine the possible photoexcitation process within the UV/vis adsorption region. Finally, we will find if there is a suitable energy match between the photoexcited electronic states in the adsorbed InN and the unoccupied electronic states around the lowest conduction band of the $TiO_2$ anatase (101) surface to provide the effective channel for electron injection through the InN/$TiO_2$ interface. After the adsorption of InN onto the $TiO_2$ anatase (101) surface through the structural mode of InN−$O_{cn2}$, we can easily find that there are new states appearing between the band gap of the clear $TiO_2$ anatase (101) surface from our calculated PDOS of monolayer-adsorbed InN as shown in the Figure 7. Apparently, the monolayer adsorption of InN onto the $TiO_2$ anatase (101) surface will cause the reduction of the band gap from 3.2 to 1.7 eV to provide the possibility of photoexcitation at 1.7 eV (730 nm) within the UV/vis adsorption region. Therefore, the structural mode of InN−$O_{cn2}$ induces the states within the band gap of the $TiO_2$ anatase (101) surface to give rise to the photoexcitation process. However, if we compare our calculated PDOS of the $TiO_2$ anatase (101) surface layer with those of monolayer-adsorbed InN as shown in Figure 7, we immediately found that there are no suitable energy matches between the lowest unoccupied electronic states of monolayer-adsorbed InN and the unoccupied electronic states around the lowest conduction band edge of the $TiO_2$ anatase (101) surface layer. In particular, we notice that our calculated PDOS for the $TiO_2$ anatase (101) surface layer around the lowest conduction band edge are much smaller than those for monolayer-adsorbed InN. Furthermore, we found that there is very little overlap between the electronic states of the $TiO_2$ anatase (101) surface and those of monolayer-adsorbed InN. Consequently, we believe that there is almost no electronic interaction between monolayer-adsorbed InN and

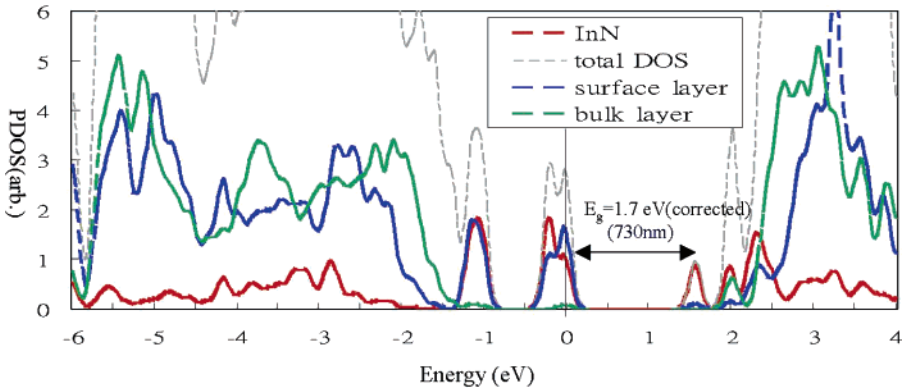


**Figure 7.** The calculated PDOS of monolayer-adsorbed InN and of both the $TiO_2$ surface and the $TiO_2$ bulk layer for InN− $O_{cn2}$ as shown by the dashed red line, dashed blue line, and dashed green line, respectively.

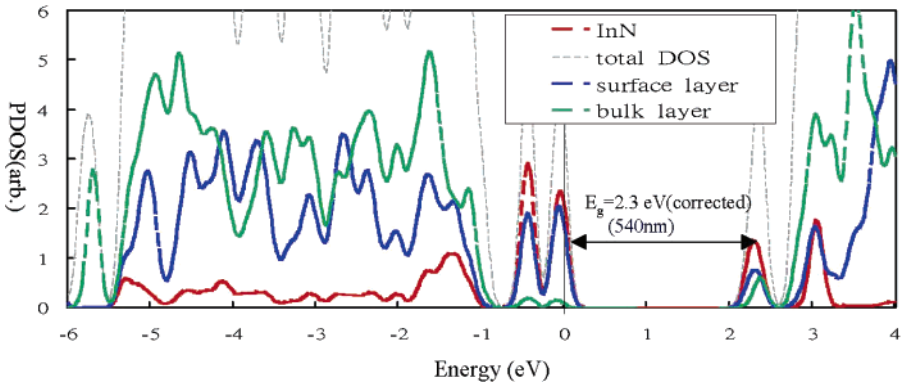


**Figure 8.** The calculated PDOS of monolayer-adsorbed InN and of both the $TiO_2$ surface and the $TiO_2$ bulk layer for $(O_{cn2})_2$−InN−$Ti_{cn5}$ as shown by the dashed red line, dashed blue line, and dashed green line, respectively.

the $TiO_2$ anatase (101) surface for this InN−$O_{cn2}$, and presumably it will not provide a feasible interfacial electron pathway for electron injection through the InN/$TiO_2$ interface.

Now let us consider our calculated PDOS of monolayer-adsorbed InN and both the surface and bulk layer of $(O_{cn2})_2$−InN−$Ti_{cn5}$ on the $TiO_2$ anatase (101) surface around the lowest conduction band edge. Again we found that there are new states appearing between the band gap of the $TiO_2$ anatase (101) surface as shown in Figure 8. Apparently, the formation of $(O_{cn2})_2$−InN−$Ti_{cn5}$ on the $TiO_2$ anatase (101) surface will cause the reduction of the band gap of the $TiO_2$ anatase (101) surface from 3.2 to 2.3 eV to provide the possibility of photoexcitation at 2.3 eV (540 nm) within the UV/vis adsorption region. In addition, our calculated PDOS for both the $TiO_2$ anatase (101) surface layer and monolayer-adsorbed InN around the lowest band edge clearly suggest that there is not only a suitable energy match but also a large overlap between the photoexcited electronic state of monolayer-adsorbed InN and the unoccupied electronic states around the lowest conduction band of the $TiO_2$ anatase (101) surface as shown in Figure 8. Furthermore, the calculated PDOS of the bulk layer of the $TiO_2$ anatase (101) surface also have a large overlap with those of both the surface layer of the $TiO_2$ anatase (101) surface and monolayer-adsorbed InN as shown in Figure 8. Consequently, we believe that the $(O_{cn2})_2$−InN−$Ti_{cn5}$ on the $TiO_2$ anatase (101) surface will be the more sensible structural mode for being used to effectively convert light into the electricity for the solar cell design. In summary, the $(O_{cn2})_2$−InN−$Ti_{cn5}$ on the $TiO_2$ anatase (101) surface is calculated to be the more feasible structural mode for photoelectro conversion compared to that of the InN−$O_{cn2}$ on the $TiO_2$ anatase (101) surface due to its better electronic interaction and energy matching between the photoexcited electronic states of monolayer-adsorbed InN and the unoccupied electronic states around the lowest conduction band edge of the $TiO_2$ anatase (101) surface.

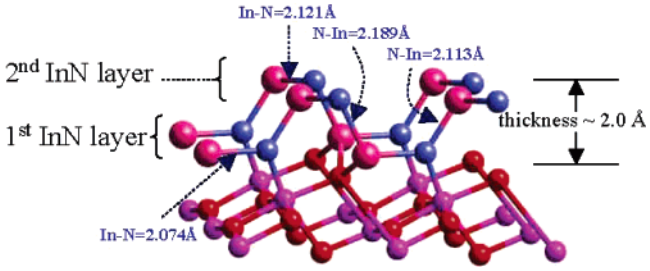


**Figure 9.** The calculated structure for double-layer-adsorbed InN on the $TiO_2$ anatase (101) surface, that is, $(O_{cn2})_2$−$(InN)_2$−$Ti_{cn5}$.

The effect of the multilayer of InN adsorbed on the $TiO_2$ anatase (101) surface on the photoexcitation followed by the electron injection through the InN/$TiO_2$ interface is another important issue worth our attention. In particular, the thickness of adsorbed InN on the $TiO_2$ anatase (101) surface is a controllable experimental parameter,[13] which will allow us to provide further insight into both photoexcitation and electron injection processes through the InN/$TiO_2$ interface. As our preliminary study, we constructed a structural model of double-layer-adsorbed InN on the $TiO_2$ anatase (101) surface, that is, $(O_{cn2})_2$−$(InN)_2$−$Ti_{cn5}$, based on the $(O_{cn2})_2$−InN−$Ti_{cn5}$ configuration and calculated its adsorption geometry and corresponding electronic properties, that is, PDOS. Our calculated, most stable structure of $(O_{cn2})_2$–$(InN)_2$−$Ti_{cn5}$ forms a stable stacking geometry in a way similar to that of the InN Würtzite crystal structure as shown in Figure 9. Our calculated band gap of this

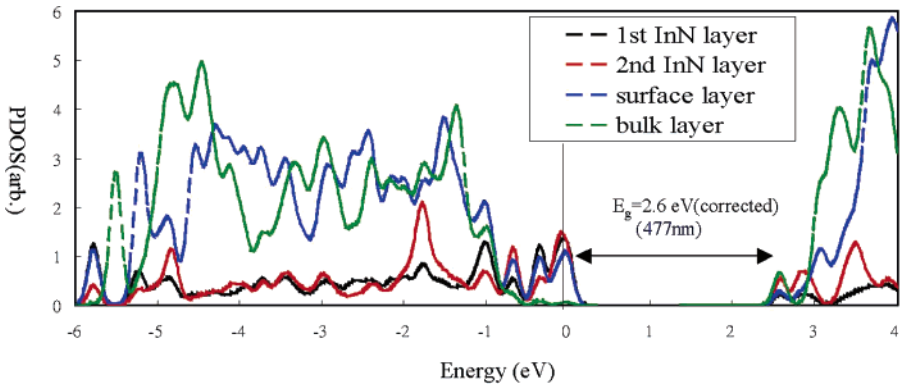


**Figure 10.** The calculated PDOS of the first adsorbed InN layer (dashed black line), the second adsorbed InN layer (dashed red line), $TiO_2$ surface (dashed blue line), and $TiO_2$ bulk layer (dashed green line) for $(O_{cn2})_2-(InN)_2-Ti_{cn5}$.

double-layer-adsorbed structure is slightly blue-shifted to 2.6 eV (477 nm) with respect to the monolayer adsorption structure. Through our analysis of calculated PDOS of both the first InN layer and the second InN layer, we found that the PDOS of these two layers are strongly coupled as shown in the Figure 10. Therefore, the electronic states of the second-layer InN can further couple with the $TiO_2$ surface through the bonding between the first-layer InN and the $TiO_2$ anatase (101) surface. In addition, we found that this double-layer-adsorbed structure has a suitable energy match and a large overlap between the photoexcited electronic state of double-layer-adsorbed InN and the unoccupied electronic states around the lowest conduction band of the $TiO_2$ anatase (101) surface very similar to that of $(O_{cn2})_2-InN-Ti_{cn5}$ side-on monolayer-adsorbed structure. Consequently, we also believe that the $(O_{cn2})_2-(InN)_2-Ti_{cn5}$ structure will be the sensible structural mode to use to effectively convert light into electricity for the solar cell design. Finally, our calculated PDOS of double-layer-adsorbed InN on the $TiO_2$ anatase (101) surface, that is, $(O_{cn2})_2-(InN)_2-Ti_{cn5}$, in comparison with those of monolayer-adsorbed InN on the $TiO_2$ anatase (101) surface, that is, $(O_{cn2})_2-InN-Ti_{cn5}$, suggest that (1) the variation of the thickness of adsorbed InN on the $TiO_2$ anatase (101) surface will change the band gap thereby to induce the photoexcitation at a different adsorption wavelength within the UV/vis region and that (2) the increasing of the thickness of adsorbed InN on the $TiO_2$ anatase (101) surface will cause the different overlap of electronic states between the top adsorbed InN layer and the bottom adsorbed InN layer and affect the effectiveness of the electron injection from adsorbed InN layer to the $TiO_2$ anatase (101) surface. In summary, on the basis of this preliminary study, we immediately realized that increasing the thickness of adsorbed InN on the $TiO_2$ anatase (101) surface would not only vary the adsorption wavelength within the UV/vis region but also change its intensity. Our results so far only could propose that the broad UV/vis absorption between 390 and 800 nm from experimental work by M. C. Lin[13] could possibly result from some mixed stable structural modes with different layers of InN adsorbed in possible different orientations on the $TiO_2$ anatase (101) surface.

## Conclusions

By combining DFT with USP and GGSA, we established the energetics and structures of monolayer-adsorbed InN on the $TiO_2$ anatase (101) surface and their corresponding electronic properties, that is, PDOS for both the surface and the bulk layer of the $TiO_2$ anatase (101) surface, and for monolayer-adsorbed InN, to shed light on the possible structural modes for initial photoexcitation within the UV/vis region followed by the electron injection through the $InN/TiO_2$ interface for the $InN/TiO_2$-based solar cell design. Our calculated adsorption energies found that both $InN-O_{cn2}$ and $(O_{cn2})_2-InN-Ti_{cn5}$ are the two most stable structural modes of monolayer-adsorbed InN on the $TiO_2$ anatase (101) surface with adsorption energies of 2.52 and 3.05 eV, respectively. Our calculated band gaps (including a 1.0-eV correction using a scissor operator) for both $InN-O_{cn2}$ and $(O_{cn2})_2-InN-Ti_{cn5}$ are red-shifted to 1.7 eV (730 nm) and 2.3 eV (540 nm), respectively. In addition, our analyses of calculated PDOS for both the surface and bulk layer of the $TiO_2$ anatase (101) surface and calculated PDOS for monolayer-adsorbed InN suggest that the $(O_{cn2})_2-InN-Ti_{cn5}$ would provide a feasible mode for initial photoexcitation followed by the electron injection through the $InN/TiO_2$ interface. This is due to the presence of occupied electronic states of monolayer-adsorbed InN within the band gap of the $TiO_2$ anatase (101) surface, which will allow the photoexcitation within the UV/vis adsorption region to take place, and subsequently these photoexcited states will overlap with the unoccupied electronic states around the lowest conduction band edge of the$TiO_2$ anatase (101) surface, which will ensure the electron injection through the $InN/TiO_2$ interface. Finally, our preliminary study of double-layer-adsorbed InN on the $TiO_2$ anatase (101) surface suggests that the effect of the increasing thickness of adsorbed InN on the $TiO_2$ anatase (101) surface on both photoexcitation and electron injection processes evolved into the photoinduced interfacial electron transfer through $InN/TiO_2$. Therefore the broad UV/vis absorption between 390 and 800 nm from experimental work by M. C. Lin would possibly be contributed by some mixed stable structural modes with different layers of InN adsorbed in different orientations on the $TiO_2$ anatase (101) surface. We are presently calculating all possible structural modes with different layers of InN adsorbed in all possible different orientations on the $TiO_2$ anatase (101) surface to gain better insight into the effect of the multilayer of InN adsorbed on the $TiO_2$ anatase (101) surface on its electronic properties of our interest.

**Acknowledgment.** The authors thank the National Science Council in Taiwan for financial support (Grant Nos. NSC93-2113-M-032-009) and Taiwan's National Center for High-Performance Computing for the use of its computational facility through the Taiwan Computational Chemistry Consortium funded by the Institute of Nuclear Energy Research Project No. NL940251. We are also grateful to Professor M. C. Lin for stimulating this research work.

## References and Notes

(1) O'Regan, B.; Gratzel, M. *Nature (London)* **1991**, *353*, 737.

(2) Nazeeruddin, M.-K.; Kay, A.; Rodicio, I.; Humphry-Backer, R.; Muller, E.; Liska, P.; Vlachopoulos, N.; Graetzel, M. *J. Am. Chem. Soc.* **1993**, *115*, 6382.
(3) Hagfeldt, A.; Gratzel, M. *Chem. Rev.* **1995**, *95*, 49.
(4) Graetzel, M. *Acc. Chem. Res.* **2000**, *33*, 269.
(5) O'Regan, B.; Graetzel, M. *Nature (London)* **2001**, *414*, 338.
(6) Liu, G.; Jaegermann, W.; He, J.; Sundstrom, V.; Sun, L. *J. Phys. Chem. B* **2002**, *106*, 5814.
(7) Huisman, C. L.; Goossen, A.; Schoonman, J. *Chem. Mater.* **2003**, *15*, 4617.
(8) Li, D.; Gu, C.; Guo, C.; Hu, C. *Chem. Phys. Lett.* **2004**, *385*, 55.
(9) Blackburn, J. L.; Selmarten, D. C.; Nozik, A. J. *J. Phys. Chem. B* **2003**, *107*, 14154.
(10) Zaban, A.; Micic, O. I.; Gregg, B. A.; Nozik, A. J. *Langmuir* **1998**, *14*, 3153.
(11) Vogel, R.; Hoyer, P.; Weller, H. *J. Phys. Chem.* **1994**, *98*, 3183.
(12) Vogel, R.; Klaus, P.; Weller, H. *Chem. Phys. Lett.* **1990**, *174*, 241.
(13) Wang, J.-H.; Lin, M. C. *ChemPhysChem* **2004**, *5*, 1615.
(14) Wang, J.-H.; Lin, M. C. *J. Phys. Chem.*, in press.
(15) Lin, J. S.; Lee, L.-F. *Int. J. Quantum Chem.* **2004**, *97*, 736.
(16) Lin, J. S.; Chou, W.-C. *J. Mol. Struct. THEOCHEM* **2003**, *635*, 115.
(17) Kresse, G.; Furthmuller, J. *Comput. Mater. Sci.* **1996**, *6*, 15.
(18) Perdew, J.; Wang, Y. *Phys. Rev. B* **1992**, *45*, 13244.
(19) Vanderbilt, D. *Phys. Rev. B* **1990**, *41*, 7892.
(20) Kleinman, L.; Bylander, D. M. *Phys. Rev. Lett.* **1982**, *48*, 1425.
(21) Monkhorst, H. J.; Pack, J. D. *Phys. Rev. B* **1976**, *13*, 5188.
(22) Segall, M. D.; Lindan, P. L. D.; Probert, M. J.; Pickard, C. J.; Hasnip, P. J.; Clark, S. J.; Payne, M. C. *J. Phys.: Condens. Matter* **2002**, *14*, 2717.